

SenSnake: A snake robot with contact force sensing for studying locomotion in complex 3-D terrain

Divya Ramesh, Qiyuan Fu and Chen Li¹

Abstract—Despite advances in a diversity of environments, snake robots are still far behind snakes in traversing complex 3-D terrain with large obstacles. This is due to a lack of understanding of how to control 3-D body bending to push against terrain features to generate and control propulsion. Biological studies suggested that generalist snakes use contact force sensing to adjust body bending in real time to do so. However, studying this sensory-modulated force control in snakes is challenging, due to a lack of basic knowledge of how their force sensing organs work. Here, we take a robophysics approach to make progress, starting by developing a snake robot capable of 3-D body bending with contact force sensing to enable systematic locomotion experiments and force measurements. Through two development and testing iterations, we created a 12-segment robot with 36 piezo-resistive sheet sensors distributed on all segments with compliant shells with a sampling frequency of 30 Hz. The robot measured contact forces while traversing a large obstacle using vertical bending with high repeatability, achieving the goal of providing a platform for systematic experiments. Finally, we explored model-based calibration considering the viscoelastic behavior of the piezo-resistive sensor, which will be useful for future studies.

Index Terms— Terradynamics, locomotion, obstacle traversal, contact

I. INTRODUCTION

Snake robots hold the promise of being a versatile platform for moving in a variety of environments for important applications [1], [2]. However, compared with the remarkable locomotor capacities of snakes in diverse 3-D terrain with large obstacles [3]–[5], snake robots are still far behind, often suffering slower speeds and larger slip [6], [7] [8]. Some snake robots use vision to scan the terrain and plan motions adapting to its geometry [8]–[13]. Others use mechanical compliance [10], [11], [14] or controlled compliance [6], [10], [15] to maintain body-surface contact. However, despite progress on how to use 2-D lateral bending to push against vertical structures on a horizontal surface to generate propulsion [16]–[19], we still do not well understand how to use 3-D body bending to push against complex 3-D terrain to do so.

An ability to sense and adjust contact forces against the terrain likely contributes to generalist snakes’ superior performance. When using 2-D lateral bending to push against vertical structures, generalist snakes can adjust their body bending in real time to maintain contact and control the direction of propulsion [4], [20], suggesting that this is a sensory-modulated process. Although it is known that snake possess both cutaneous mechanoreceptors (i.e., skin tactile sensing) and proprioceptors within the muscles and tendons (i.e., internal position, movement, and force sensing) [21]–[23], it remains unknown how these sensors are used to detect body position or environmental forces to control locomotion.

*This work was supported by an Arnold and Mabel Beckman Foundation Beckman Yong Investigators Award, a Burroughs Wellcome Fund Career Award at the Scientific Interface, a Johns Hopkins University Catalyst Award, and the JHU Whiting School of Engineering start-up funds to C.L.

Such a lack of basic knowledge makes it difficult to study snakes to understand how to sense and control contact forces to generate propulsion in complex 3-D terrain.

Robots have proven very useful as physical models of animals for studying locomotion, especially in complex environments, where it is difficult or impossible to create tractable theoretical models [24]–[27]. In addition, contact force measurements [28] have advanced understanding and performance of many aspects of locomotion and manipulation tasks, including object identification [29], slip detection [30], tactile sensing [31], [32], exploring and interacting with cluttered environments [33], and terrain identification and classification [34], [35]. Here, to establish a platform for studying the physical principles of sensing and controlling contact forces to generate propulsion in complex 3-D terrain and ultimately improve snake robot performance, we developed a snake robot, SenSnake, capable of 3-D body bending with contact force sensing along its body.

We first developed and tested an initial robot prototype (Sec. II). Based on limitations revealed, we refined the robot and sensor design (Sec. III). This enabled the robot to move over a large obstacle and measure contact forces with high repeatability (Sec. III), achieving our major goal of providing a robotic platform for systematic experiments (rather than optimizing robot performance as in many robotics studies). In addition, we performed experiments to calibrate the sensors on the refined robot, which can improve the accuracy of force estimates and inform future design of terrain testbeds for studying complex 3-D terrain traversal (Sec. IV). Finally, we summarize our contributions and discuss future directions (Sec. V).

II. INITIAL SENSOR & ROBOT DEVELOPMENT

A. Initial robot prototype

The initial robot prototype, SenSnake v1 (0.9 m long, 0.044 m cross-sectional radius, 4.6 kg), had 12 alternating pitch and yaw segments to bend in three dimensions (Fig. 1A). Each segment had a servo motor (Dynamixel XM450-W350R) fully enclosed in a soft shell casted from silicone (Ecoflex 00-30, Smooth-On Inc.) (Fig. 1C, black) attached via 3-D printed shell holders (Fig. 1C). On the outside of the soft shell, each pitch segment had an array of four sensors (in a 2×2 arrangement) on its bottom, whereas each yaw segment had two such arrays on both sides (Fig. 1D). This resulted in a total of 72 sensors, which could be recorded at a sampling frequency of 17 Hz (see Sec. II, D). The soft shell was intended to deform passively during terrain interaction to

¹Department of Mechanical Engineering, Johns Hopkins University, Baltimore, MD 21218 USA (e-mail: dramesh@jhu.edu, fqiuyuan1@jhu.edu, chen.li@jhu.edu). Corresponding author: Chen Li.

improve terrain-sensor contact.

The robot was powered with using an external 12 V DC supply. The motors were daisy-chained and controlled using a USB communication convertor (U2D2, Dynamixel). A rubber layer was added over each sensor to prevent sensor wear and tear (Fig. 1B). A PolyEthylene Terephthalate braided sleeve (Flexo Pet, Techflex) was added over the robot to reduce friction. Eighteen 8 pin FFC cable adapter to 8 DIP adapter PCB boards (chipboards, green blocks in Fig. 1A) were attached to the top part of the shell holder to connect sensors to a Data Acquisition board (DAQ).

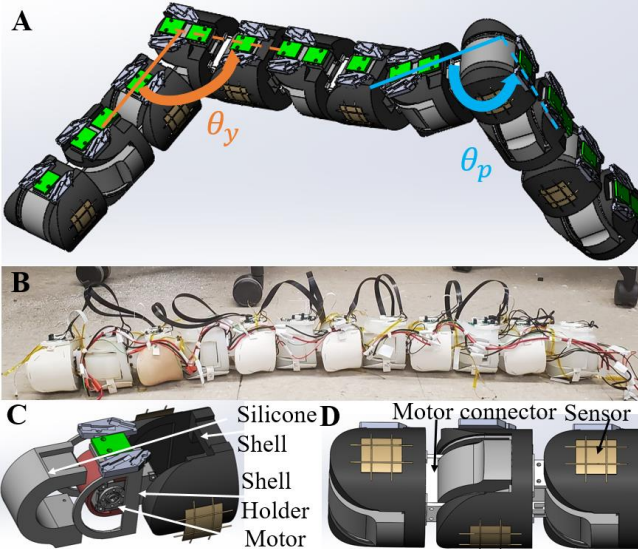


Figure 1. SenSnake v1. (A) CAD showing 3-D bending with pitch and yaw degrees of freedom. (B) Photo of robot without sleeve. (C) Exploded view of a segment. (D) Side view CAD of three segments with sensors on the side of yaw and bottom of pitch segments.

B. Choice of sensors

We needed small sensors that can be custom made to the desired shape to fit on the outside of the robot body for directly sensing terrain contact. In addition, because body compliance helps passively adapt to 3-D terrain to improve contact [11], the sensors should also be flexible. Furthermore, a large number of sensors were necessary for the robot to be able to sense contact distributed on the many segments. Commercial high quality strain gauge-based, multi-axis force/torque sensors have high accuracy but are bulky, expensive, and delicate. Off-the-shelf, low-cost piezo-resistive sensors [16], [18], [19], [36] or custom made force sensors [37], [38] have been used in previous snake robots with great success. The custom made sensors used in [37] use strain gauges that can become expensive when used in large numbers; those in [38] are more complex in design and use rigid components that are more susceptible to damage. Considering these, we chose to use a custom piezo-resistive sensor design [29], [39].

C. Sensor fabrication

The sensor array consisted of seven layers (Fig. 2A). A piezo-resistive film (3M Velostat, 0.1 mm thickness, Adafruit Industries) was sandwiched between parallel stainless steel conductive threads (3 ply, 0.25 mm thickness, Adafruit Industries) above and below, which were perpendicular each

other (Fig. 2A). Each crossing of threads above and below forms a single sensor. An adhesive sheet (Gizmo Dorks 468MP, 2.54 mm thickness, 3M) was placed over the conductive threads on either side (Fig. 2A) and adhered to the piezo-electric film, followed by a sheet of plastic wrap.

Each sensor experiences a reduction in resistance R_s on application of normal force. The sensor conductance, $G_s = 1/R_s$, increases linearly with the force applied (Fig. 2B):

$$G_s = mF + d \quad (1)$$

where m and d are constants. See multimedia material part 1 for a demonstration of sensor operation.

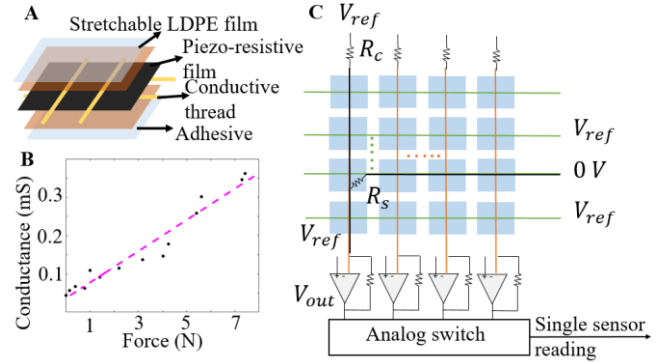


Figure 2. Sensor fabrication, calibration, and data acquisition. (A) Piezo-resistive sensor design. (B) Measured conductance as a function of force applied. Dashed line is best linear fit. (C) Signal isolation circuit used to collect the sensor readings. Blue squares are piezo-resistive sheets.

D. Sensor data acquisition

To obtain sensor data, we replicated the DAQ designed in [29], which scans through sensors one at a time using a multiplexer and a demultiplexer (Fig. 2C). The DAQ also uses a signal isolation circuit to minimize sensor crosstalk, an undesirable effect that sensors close to each other affect each other's resistance [40].

We characterized the sampling frequency of the DAQ, defined as the frequency at which data from all sensors being tested can be received. As expected, sampling frequency decreased monotonically with the number of sensors (Fig. 3A), starting at about 20 Hz for one sensor, decreasing to 10 Hz for ~ 300 sensors, and approaching only a few Hz for ~ 1000 sensors. When two DAQ were used, sampling frequency decreased but only slightly (Fig. 3B).

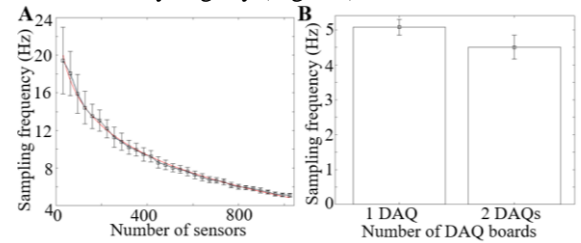


Figure 3. Sampling frequency of sensor data acquisition (mean \pm s.d. of 100 trials). (A) Sampling frequency as a function of the number of sensors. (B) Comparison of sampling frequency between one and two DAQ used. 1024 sensors were scanned for each case.

E. Experiments and issues revealed

We tested SenSnake v1 on flat rigid ground and a pile of small wooden blocks using lateral undulation (15.24 cm long,

5.08 cm wide, 3.38 cm tall; Fig. 4A-B). In both cases, the robot did not progress forward due to a lack of anisotropic friction necessary for moving on smooth flat surfaces using lateral undulation [41]. We observed constant forces when the robot remained stationary for the first 10 s (Fig. 4C-D). During lateral undulation, force data oscillated periodically on flat ground (Fig. 4C) and not so regularly on blocks (Fig. 4D). These results showed that the sensors can detect the expected forces during locomotion. See multimedia material part 3 for an example video.

However, these tests also revealed several issues. First, we observed small signals on a large portion of the force sensors on the body segments in contact with the block pile. This suggested that the silicone shell did not deform sufficiently to distribute highly localized stresses at terrain contact points widely to reach the exact locations of the sensors. Because each sensor covered only a small area at the crossing of the perpendicular conductive threads, it could not detect a large force signal. In addition, contrary to expectation, the differences between the four sensors within each 2×2 sensor array on the block pile were similar to those on flat ground (Fig. 4C-D). This was likely a result of the lack of direct contact at the sensor point. This further showed that the intended high sensor spatial resolution did not outweigh the limitation from the small sensor area. Moreover, some of the sensors developed substantially noisy reading during experiments (Sensors 3R, 4B, 11L in Fig. 4C-D). Examination of the robot and further testing revealed that these sensor wires became loose at the sensor-chipboard connection during experiments.

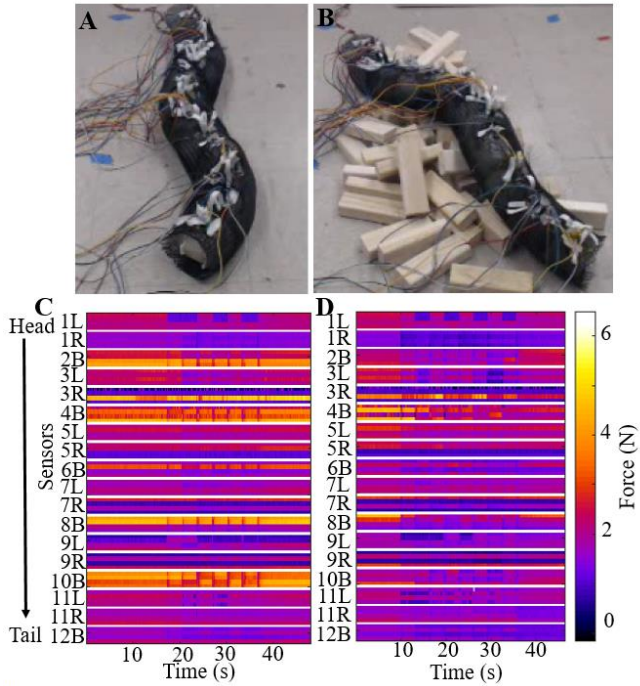


Figure 4. Initial robot prototype experiment. (A) Lateral undulation on flat ground. (B) Lateral undulation on rubble of wooden blocks. (C) Force readings varying with time on flat ground. (D) Force readings varying with time on rubble of wooden blocks. 1L indicates 1st segment left, 1R indicates 1st segment right and 2B indicates 2nd segment bottom.

We also tested the robot to traverse a single large obstacle as high as $0.28 \times$ robot length by propagating a vertical bending

shape that conforms to the obstacle down its body, a strategy inspired by recent animal observations [42]. Although the robot was able to generate the desired shape evolution on its own, it failed to use it against the large obstacle to propel forward. Examination of motor angle data revealed that the motors could not reach the desired positions during obstacle interaction. This was likely because pushing against the large obstacle resulted in high contact forces concentrated on segments contacting the forward half of the obstacle. To propel the entire robot forward, these segments must sustain these large contact forces to overcome the large frictional drag from the substantial weight of the robot from the silicone layers. This large force requirement, together with restrictions from the sleeves, probably resulted in motor overload and triggered motor to give to prevent damage.

III. REFINED SENSOR & ROBOT DEVELOPMENT

We made several design and fabrication improvements to address these issues in a refined robot using refined sensors. These include: (1) replacing the silicone shell with a more compliant, hollow shell to reduce robot weight and sleeve restriction and improve body/sensor-terrain conformation; (2) replacing each 2×2 sensor array with a single sheet sensor [39] for more reliable force detection, which further allows increasing sampling frequency; (3) adding a sensor to the left, right, and bottom sides of each segment to improve overall body sensor coverage; and (4) embedding wiring inside the robot to minimize disturbance during locomotion..

A. Refined sensors

We switched to a piezo-resistive sheet sensor to reduce the number of sensors to improve wire packaging and increase the sensor contact area. The sheet sensor used in the improved robot is similar in design to the sensor array, except that the conductive threads (Fig. 2A) were replaced with a copper conductive sheet (Copper foil sheet with conductive adhesive, 0.07 mm thickness, Adafruit Industries) on either side (Fig. 5A). The working principle of the sheet sensor is the same as the sensor array.

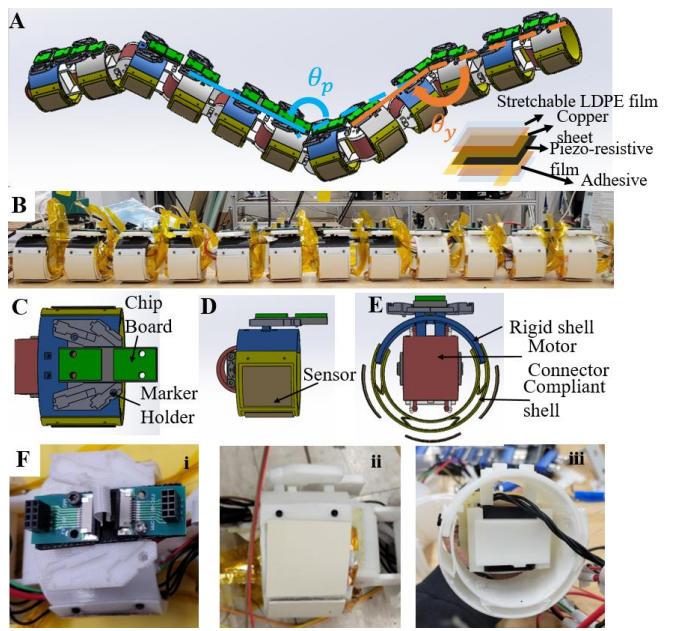


Figure 5. SenSnake v2 design. (A) CAD showing 3-D bending of

robot. (B) Photo of robot. (C-E) Top, side, and front views of a segment CAD. (F) Top (i), side (ii) and front view (iii) photos of a segment.

B. Refined robot

The refined robot, SenSnake v2 (0.96 m long, XX m segment radius, 2.4 kg), also consists of 12 segments (Fig. 5B) and has the same joint structures as the initial robot (Fig. 5A). To make the robot lighter, the silicone shell was replaced with a compliant, hollow shell to evenly distribute the force on the sensor (Fig. 5E). Because only the sides and bottom of the robot came in contact with the terrain obstacles during traversal, the upper part of the shell was 3-D printed using PLA for rigidity (Fig. 5C, blue) whereas the rest of the shell was 3-D printed soft using TPU (Fig. 5D, yellow). The piezo-resistive sheet sensors were placed over a maximum area on the soft part of the shell to detect contact forces.

Three sensors (4 cm long and 3.5 cm wide) were distributed over the soft shell (Fig. 5E) to detect the forces on left, right and bottom of each segment, totaling 36 sensors with a sampling frequency of 30 Hz. Each sensor was covered by a rubber layer to prevent wear and tear of the sensor (Fig. 5Fii). We improved wiring to be enclosed inside the shell for better protection (Fig. 5Fi, 5Fiii). We further installed 3-D printed holders to mount LED motion capture markers to track each segment of the robot.

C. Experiments

To test how well our sensor and robot improvements solved the problems in the initial prototype and demonstrate the usefulness of using it to understand locomotion in complex terrain, we tested the refined robot on wooden half-cylindrical obstacle constructed from assembling laser cut boards (Fig. 6A-B). To reduce friction, we covered the entire surface with plastic sheet (0.254 mm polytetrafluoroethylene sheet, McMaster, USA). Eight motion capture cameras (PhaseSpace IMPULSE X2) tracked 4 unique LED markers on each segment to obtain 3-D kinematics at 960 Hz (Fig. 5C).

We used feedforward control using Robot Operating System at a frequency of 50 Hz to propagate a pre-defined vertical bending shape down the body at 0.034 rad/s in a follow-the-leader manner. This pre-defined shape was generated by manually pushing the robot down to conform to the obstacle and recording the motor angles. The controller used linear interpolation of motor angles over time to propagate the shape down the body. The robot started with the 6th segment on top of middle of the obstacle, because on a flat ground a vertical bending could not generate sufficient propulsion to move it forward.

Overall, the robot conformed well to the obstacle and generated sufficient propulsion to propel itself forward to traverse the large obstacle. As the robot moved forward, all the contact forces patterns propagated backward relative to the robot (Fig. 7C). For the first 10 seconds after the robot started moving, forward motion was smooth (Fig. 7Ai), with substantial normal forces (~5 N, ~22% robot weight) the segments contacting the front of the obstacle and the horizontal surface (Fig. 7Ci). Besides supporting part of the robot weight, the normal force against the front side of the obstacle also resulted in forward propulsion.

Until the middle of the robot passed over the middle of the

obstacle (Fig. 7Ai), the robot slowed down momentarily on the obstacle, presumably due to a relative contact. As the robot continued to propagate bending backward, the segment contacting the front side of the obstacle pushed harder and generated a very large force (23 N, 98% robot weight) (Fig. 7ii). This buildup of forward propulsion eventually helped the robot overcome frictional drag and slip forward rapidly, after which it resumed steady motion (Fig. 7iii-iv). See multimedia material part 4 for an example video.

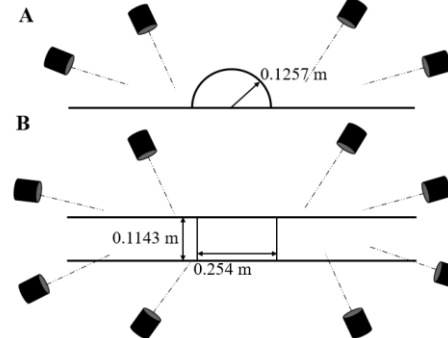


Figure 6. Experimental setup. (A, B) Side view schematic. (B) Top view schematic. The black cylinders are motion capture cameras.

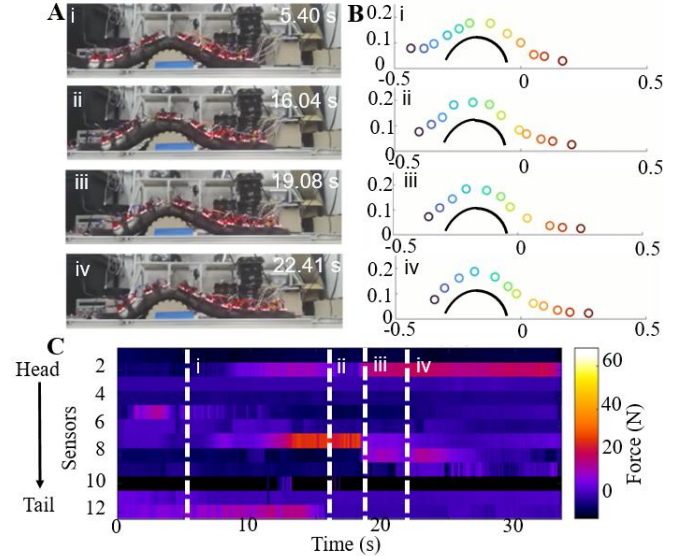


Figure 7. Robot feedforward control. (A) Side view snapshots of robot traversing a large half-cylindrical obstacle. (B) Side view reconstruction of segment positions from motion capture data. (C) Measured force as a function of time for all sensors on the bottom of the robot. White lines in B correspond to snapshot times in A.

We performed three trials and found excellent repeatability in the robot's motion and sensor data (Fig. 8A-B), achieving our main goal of providing a robotic platform for systematic experiments to understand the physical principles of locomotion [24]–[27].

IV. MODEL-BASED SENSOR CALIBRATION

With proper design and fabrication, piezo-resistive force sensors enabled our snake robot to detect contact forces when traversing large obstacles. This is consistent with previous success in snake robots doing so against large vertical structures on flat surfaces [16]. One distinction is that these previous studies focused mainly on using sensor data to generate locomotion in a robot. Our robot sensor development

is not only to help generate locomotion, but also to provide quantitatively accurate measurements necessary for understanding the physical principles of snake propulsion generation using 3-D body bending.

Considering this additional need, we must take into account of the viscoelastic nature of piezo-resistive material, which causes a creep behavior of the sensor reading after an application of force [43]. Thus, we carried out further sensor modeling and calibration experiments to provide high-fidelity force information from sensing reading, following recent work [39].

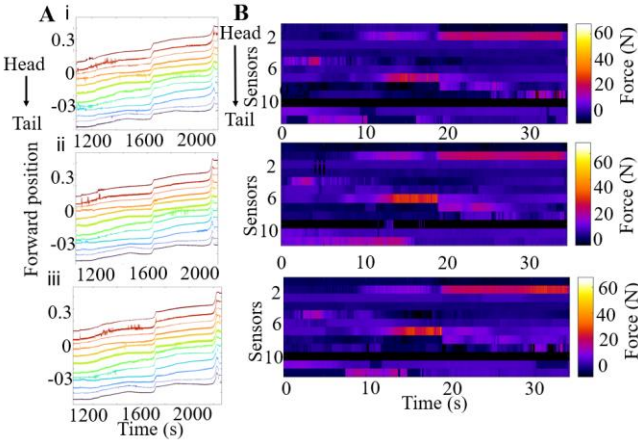


Figure 8. High system repeatability for robophysics studies. (A) Segment forward position as a function of time. (B) Force as a function of time for all bottom sensors.

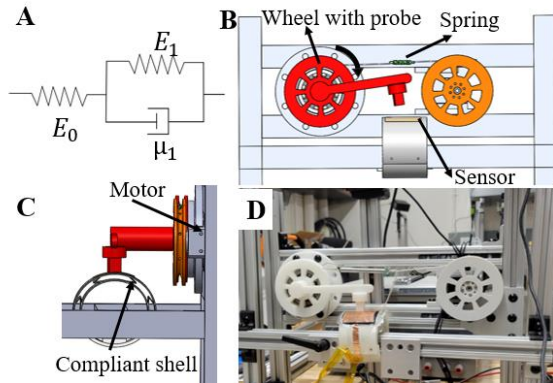


Figure 9. Calibration setup. (A) Sensor model. (B, C) Side and front view schematics of calibration setup. (D) Front view photo of calibration setup.

A. Sensor model

Various models have been developed to model creep behaviors in viscoelastic materials under a constant stress [43]. Simpler models such as Maxwell model does not estimate creep accurately and the Kelvin-Voigt model, another simpler model, is less accurate for modeling relaxation. The kelvin representation of the 3-parameter model which we used in this study well describes both creep and relaxation.

Here, we follow the approach developed for modeling creep in piezo-resistive material [39], which adopts the Kelvin representation of the standard linear solid model (Fig. 9A) and captures the physical mechanisms of how stress leads to sensor deformation [43] which further leads to resistance change [39].

The dynamics of the model is given by:

$$\sigma + \frac{\mu_1}{E_0+E_1} \dot{\sigma} = \frac{E_0 E_1}{E_0+E_1} \varepsilon + \frac{\mu_1 E_0}{E_0+E_1} \dot{\varepsilon} \quad (2)$$

where $\sigma = F/A$ the stress applied, ε is the induced strain, E_0 and E_1 are the elastic coefficients and μ_1 is the viscos coefficients of the piezo-resistive material, F is the force applied, and A is the active area of the sensor that is being deformed. Note that E_0 , E_1 , and μ_1 are model fitting parameters that linearly increase with the force applied [39], not constant material properties.

The resistance-strain relationship is:

$$R_s = \frac{\rho_1 + \rho_2}{2} \sqrt{\frac{\pi H}{F}} + R_0 (1 - \varepsilon) e^{-\gamma D \varepsilon \left[\left(\frac{\pi}{6\phi} \right)^{\frac{1}{3}} - 1 \right]} \quad (3)$$

where R_s is the total resistance measured, ρ_1 and ρ_2 are the resistivities of the piezo-resistive and conductive materials, respectively, H is the hardness of the material that measures the resistance of a material to localized plastic deformation, R_0 is the initial resistance of the piezo-resistive material, D is the filler particle diameter, and ϕ is the volume fraction of the filler particles. γ is defined by:

$$\gamma = \frac{4\pi}{h} \sqrt{2m_e \varphi} \quad (4)$$

where h is the Plank's constant, m_e is the mass of an electron, and φ is the height of the potential barrier between the two adjacent filler particles.

B. Model parameter estimation

Three sensor model parameters E_0 , E_1 and μ_1 are estimated using the least squares parameter estimation method [44]. For a given constant force, the resistance R_s is found using the DAQ board readings. The strain ε is then estimated using the Eq. 3. The stress-strain dynamics in Eq. 2 can be rewritten as:

$$\sigma + a\dot{\sigma} = b\varepsilon + c\dot{\varepsilon} \quad (5)$$

where:

$$a = \frac{\mu_1}{E_0+E_1}, \quad b = \frac{E_0 E_1}{E_0+E_1}, \quad c = \frac{\mu_1 E_0}{E_0+E_1} \quad (6)$$

The stress-strain system can be further rearranged:

$$\sigma = \phi\theta \quad (7)$$

where ϕ is defined as follows:

$$\phi = [\varepsilon \quad \dot{\varepsilon} \quad -\dot{\sigma}] \quad (8)$$

If ϕ is a non-singular matrix, then the following equation can be used to estimate Θ :

$$\hat{\Theta} = (\phi^T \phi)^{-1} \phi^T \sigma \quad (9)$$

The estimated parameters can then be found using Eq. 8 where:

$$\hat{\Theta} = [\hat{b} \quad \hat{c} \quad \hat{a}]^T \quad (10)$$

The conductance measured in the trials were used to estimate the strain. The conductance after the creep behavior were plotted against force to find the fitting parameters. The linear relationship between the force applied and the conductance was used to find the fitting parameters.

C. Calibration setup

We developed a calibration system to calibrate the sensors systematically and repeatedly. A servo motor rotates a 3-D printed wheel (Fig. 9B, orange), which tries to rotate another wheel through a cable with a spring (stiffness = 246 N/m) to push a probe against the sensor. The spring allows the pushing

wheel (Fig. 9B, red) to stop rotating while generating a controlled force that can be measured by measuring spring deformation. During calibration, we attached a fully assembled segment onto an aluminum beam and actuated the motor to apply a constant force for 370 s at a sampling frequency of 6 Hz. We tested four different constant forces, 1.75, 3, 4 and 5.25 N, and collected 3 trials each. See multimedia material part 2 for a demonstration of the setup.

D. Choice of calibration probe

In complex 3-D terrain, the robot may push against various objects, resulting in flat surface contact (Fig. 10A-B), edge contact (e.g., Fig. 10C), and corner contact (Fig. 10D). These diverse contact conditions may affect the repeatability of the sensors and fidelity of sensor model, but few studies considered their effects [39], [45]. To test how robust our sensors and model-based calibration is, we tested four probes. A large flat probe covering the entire sensor simulates a flat surface contact (Fig. 10A). A small flat probe simulates a flat surface contact with edges (Fig. 10B). A sharp edge probe simulates an edge contact (Fig. 10C). A multi-point probe simulates point contacts (Fig. 10D).

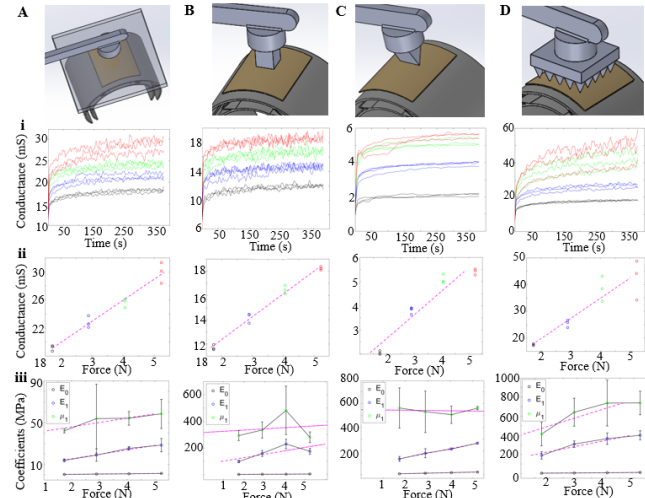


Figure 10. Model-based sensor calibration results. (A) Large flat probe. (B) Small flat probe. (C) Sharp edge probe. (D) Multi-point probe. (i) Measured sensor conductance as a function of time for four different constant forces. (ii) Average conductance after 300 s using data in (i) as a function of applied force. (iii) Sensor parameters from model fitting as a function of applied force. The dashed lines in (i) and (iii) indicate linear fit lines. Black, blue, green, and red are for applied forces of 1.75, 3, 4, and 5.25 N.

For the large flat probe, all the three estimated parameters increased linearly with force (Fig. 10Aiii), consistent with previous observations [39]. However, for the small flat, sharp edge and multi-point probes, this was not the case (Fig. 10iii). Close observations of probe-sensor interaction during calibration showed that the local shape of the contact area changed significantly (see multimedia material part 5). We also found that piezo-resistive layer of the sensor was creased and damaged after repeated calibration tests.

These observations are informative for our future systematic robophysics experiments. To ensure high-fidelity force data to gain principled understanding of locomotion in complex 3-D terrain, it would be more practical to design

terrain testbeds with large obstacles that are sufficiently smooth to minimize edge or corner contact to repeatable sensor data whose behaviors can be well described by the sensor model. Certainly, sensors more robust to such contacts inevitable in the real world still need to be developed for robotic applications.

We note that, even though contact forces during locomotion change dynamically at a time scale comparable or even smaller than the sensor creep time scale, we expect that the sensor model can be used to recover the dynamic forces from the sensor signals, as long as the sensor model offers a good approximation of the actual sensor mechanics. This is because: (1) Sensor strain can be retrieved from sensor resistance (Eq. 3). (2) The stress-strain model is a second-order system that is observable (Eq. 2).

The plausibility of this expectation is further evidenced by the literature. Many previous studies, ranging from snake robots[18], [36], legged robots[34], [35], to wheeled vehicles [46], used piezo-resistive force sensors with viscoelastic responses that occur at the same or even a longer time scale as the dynamic locomotion process being measured. Despite not considering the complexity of sensor reading changes from viscoelastic response, these studies were successful in achieving the intended sensor function in locomotion (e.g., terrain classification, obstacle traversal, navigation). For our goal of understanding locomotion principles, it is important to obtain accurate dynamic force information. We will explore how to use the sensor model to do this in future work.

An intriguing question is whether biological organisms like snakes, with cutaneous mechanoreceptors and proprioceptors within viscoelastic skins, muscles, and tendons [21]–[23], have somehow solved this problem through evolution.

V. SUMMARY & FUTURE WORK

To provide a platform for studying how to use contact force sensing to modulate 3-D body bending to propel against 3-D terrain for locomotion, we developed a snake robot with contact force sensors distributed along its entire body. Through two development and testing iterations, our robot was able to obtain contact force measurements while moving over a large obstacle with high repeatability required for systematic studies. Our next step in robot development is to add feedback control using force information from the sensors, so that the robot can adjust body bending to better conform to and push against complex 3-D terrain [47]. Our next step in sensor calibration is to study how to use the sensor model and estimated sensor parameters to estimate dynamic forces during locomotion.

ACKNOWLEDGMENT

We thank Nikhil Murty for help with early sensor development, Kaiwen Wang for early robot design, Yaqing Wang for calibration setup development, and Yaqing Wang, Ratan Othayoth, and Henry Astley for discussion. Author contributions: D.R. developed robot, conducted experiments, and analyzed data. Q.F. developed robot control and assisted in robot design and experimental setup. D.R. and C.L. wrote the paper with input from Q.F.

REFERENCES

[1] I. D. Walker, H. Choset, and G. S. Chirikjian, *Snake-like and continuum robots*. Springer, 2016.

[2] P. Liljebeck, K. Y. Pettersen, Ø. Stavdahl, and J. T. Gravdahl, “A review on modelling, implementation, and control of snake robots,” *Rob. Auton. Syst.*, vol. 60, no. 1, pp. 29–40, 2012.

[3] S. W. Gart, T. W. Mitchel, and C. Li, “Snakes partition their body to traverse large steps stably,” *J. Exp. Biol.*, vol. 222, no. 8, 2019.

[4] P. E. Schiebel, A. M. Hubbard, and D. I. Goldman, “Comparative study of snake lateral undulation kinematics in model heterogeneous terrain,” *Integr. Comp. Biol.*, 2020.

[5] Q. Fu, S. W. Gart, T. W. Mitchel, J. S. Kim, G. S. Chirikjian, and C. Li, “Body lateral deformation and compliance help snakes and snake robots stably traverse large steps,” *Integr. Comp. Biol.*, vol. 60.

[6] T. Wang, J. Whitman, M. Travers, and H. Choset, “Directional Compliance in Obstacle-Aided Navigation for Snake Robots,” *Proc. Am. Control Conf.*, vol. 2020-July, pp. 2458–2463, 2020.

[7] J. Liu, Y. Tong, and J. Liu, “Review of snake robots in constrained environments,” *Rob. Auton. Syst.*, vol. 141, p. 103785, 2021.

[8] M. Tanaka and K. Tanaka, “Climbing and descending control of a snake robot on step environments based on kinematics,” *IEEE Int. Conf. Intell. Robot. Syst.*, pp. 3285–3290, 2013.

[9] L. Pfotzer, M. Staehler, A. Hermann, A. Roennau, and R. Dillmann, “KAIRO 3: Moving over stairs & unknown obstacles with reconfigurable snake-like robots,” *2015 Eur. Conf. Mob. Robot. ECMR 2015 - Proc.*, pp. 3–8, 2015.

[10] T. Takemori, M. Tanaka, and F. Matsuno, “Gait Design for a Snake Robot by Connecting Curve Segments and Experimental Demonstration,” *IEEE Trans. Robot.*, vol. 34, no. 5, pp. 1384–1391, 2018.

[11] Q. Fu and C. Li, “Robotic modelling of snake traversing large, smooth obstacles reveals stability benefits of body compliance,” *R. Soc. Open Sci.*, vol. 7, no. 2, 2020.

[12] T. Takemori, M. Tanaka, and F. Matsuno, “Hoop-Passing Motion for a Snake Robot to Realize Motion Transition Across Different Environments,” *IEEE Trans. Robot.*, pp. 1–16, 2021.

[13] M. Nakajima, M. Tanaka, K. Tanaka, and F. Matsuno, “Motion control of a snake robot moving between two non-parallel planes,” *Adv. Robot.*, vol. 32, no. 10, pp. 559–573, 2018.

[14] H. Kimura and S. Hirose, “Development of Genbu: Active wheel passive joint articulated mobile robot,” *IEEE Int. Conf. Intell. Robot. Syst.*, vol. 1, no. October, pp. 823–828, 2002.

[15] M. Travers, J. Whitman, and H. Choset, “Shape-based coordination in locomotion control,” *Int. J. Rob. Res.*, vol. 37, no. 10, pp. 1253–1268, 2018.

[16] T. Kano and A. Ishiguro, “Obstacles are beneficial to me! Scaffold-based locomotion of a snake-like robot using decentralized control,” *IEEE Int. Conf. Intell. Robot. Syst.*, pp. 3273–3278, 2013.

[17] A. Dinesh, H. Goldfarb, D. Sarrico, C. Scanlon, S. Hyun Yoo, and A. Mazzeo, “Applications of E-textile Pressure Sensors,” 2017.

[18] T. Kamegawa, T. Akiyama, Y. Suzuki, T. Kishutani, and A. Gofuku, “Three-Dimensional Reflexive Behavior by a Snake Robot with Full Circumference Pressure Sensors,” *Proc. 2020 IEEE/SICE Int. Symp. Integr. SII 2020*, pp. 897–902, 2020.

[19] P. Liljebeck, K. Y. Pettersen, Ø. Stavdahl, and J. T. Gravdahl, “Experimental Investigation of Obstacle-Aided,” vol. 27, no. 4, pp. 792–800, 2011.

[20] T. Kano, T. Sato, R. Kobayashi, and A. Ishiguro, “Local reflexive mechanisms essential for snakes’ scaffold-based locomotion,” *Bioinspiration and Biomimetics*, vol. 7, no. 4, 2012.

[21] M. Von During, “Sensory nerve endings of the skin and deeper structures,” *Biol. Reptil. Neurol. A*, vol. 9, pp. 407–441, 1979.

[22] A. Crowe, “Muscle spindles, tendon organs, and joint receptors,” *Sensorimotor Integr. Chicago Univ. Chicago Press*, p. pp. 454–95, 1992.

[23] J. M. Crowe-Riddell, R. Williams, L. Chapuis, and K. L. Sanders, “Ultrastructural evidence of a mechanosensory function of scale organs (sensilla) in sea snakes (Hydrophinae),” *R. Soc. Open Sci.*, vol. 6, no. 4, 2019.

[24] J. Aguilar *et al.*, “A review on locomotion robophysics: The study of movement at the intersection of robotics, soft matter and dynamical systems,” *Reports Prog. Phys.*, vol. 79, no. 11, 2016.

[25] A. J. Ijspeert, “Biorobotics: Using robots to emulate and investigate agile locomotion,” *Science (80-.).*, vol. 346, no. 6206, pp. 196–203, 2014.

[26] J. Long, *Darwin’s devices: what evolving robots can teach us about the history of life and the future of technology*. Basic Books (AZ), 2012.

[27] N. Gravish and G. V. Lauder, “Robotics-inspired biology,” *J. Exp. Biol.*, vol. 221, no. 7, pp. 1–8, 2018.

[28] P. Roberts, M. Zadan, and C. Majidi, “Soft Tactile Sensing Skins for Robotics,” *Curr. Robot. Reports*, vol. 2, no. 3, pp. 343–354, 2021.

[29] S. Sundaram, P. Kellnhofer, Y. Li, J. Y. Zhu, A. Torralba, and W. Matusik, “Learning the signatures of the human grasp using a scalable tactile glove,” *Nature*, vol. 569, no. 7758, pp. 698–702, 2019.

[30] Y. Wang, X. Wu, D. Mei, L. Zhu, and J. Chen, “Flexible tactile sensor array for distributed tactile sensing and slip detection in robotic hand grasping,” *Sensors Actuators, A Phys.*, vol. 297, p. 111512, 2019.

[31] G. Yao *et al.*, “Bioinspired Triboelectric Nanogenerators as Self-Powered Electronic Skin for Robotic Tactile Sensing,” *Adv. Funct. Mater.*, vol. 30, no. 6, pp. 1–9, 2020.

[32] M. Zhu, M. Lou, I. Abdalla, J. Yu, Z. Li, and B. Ding, “Highly shape adaptive fiber based electronic skin for sensitive joint motion monitoring and tactile sensing,” *Nano Energy*, vol. 69, no. January, p. 104429, 2020.

[33] A. Gruebele, J. P. Roberge, A. Zerbe, W. Ruotolo, T. M. Huh, and M. R. Cutkosky, “A stretchable capacitive sensory skin for exploring cluttered environments,” *IEEE Robot. Autom. Lett.*, vol. 5, no. 2, pp. 1750–1757, 2020.

[34] J. J. Shill, E. G. Collins, E. Coyle, and J. Clark, “Terrain identification on a one-legged hopping robot using high-resolution pressure images,” *Proc. - IEEE Int. Conf. Robot. Autom.*, pp. 4723–4728, 2014.

[35] X. A. Wu, T. M. Huh, A. Sabin, S. A. Suresh, and M. R. Cutkosky, “Tactile Sensing and Terrain-Based Gait Control for Small Legged Robots,” *IEEE Trans. Robot.*, vol. 36, no. 1, pp. 15–27, 2020.

[36] P. Liljebeck, K. Y. Pettersen, and Ø. Stavdahl, “A snake robot with a contact force measurement system for obstacle-aided locomotion,” *Proc. - IEEE Int. Conf. Robot. Autom.*, pp. 683–690, 2010.

[37] P. Liljebeck, Ø. Stavdahl, K. Y. Pettersen, and J. T. Gravdahl, “A modular and waterproof snake robot joint mechanism with a novel force/torque sensor,” *IEEE Int. Conf. Intell. Robot. Syst.*, pp. 4898–4905, 2012.

[38] M. Shimojo, T. Araki, S. Teshigawara, A. Ming, and M. Ishikawa, “A net-structure tactile sensor covering free-form surface and ensuring high-speed response,” *IEEE Int. Conf. Intell. Robot. Syst.*, pp. 670–675, 2007.

[39] M. Kalantari, J. Dargahi, J. Kövecses, M. G. Mardasi, and S. Nouri, “A new approach for modeling piezoresistive force sensors based on semiconductive polymer composites,” *IEEE/ASME Trans. Mechatronics*, vol. 17, no. 3, pp. 572–581, 2012.

[40] T. D’Alessio, “Measurement errors in the scanning of piezoresistive sensors arrays,” *Sensors Actuators, A Phys.*, vol. 72, no. 1, pp. 71–76, 1999.

[41] D. L. Hu, J. Nirody, T. Scott, and M. J. Shelley, “The mechanics of slithering locomotion,” *Proc. Natl. Acad. Sci. U. S. A.*, vol. 106, no. 25, pp. 10081–10085, 2009.

[42] D. J. Jurestovsky, L. R. Usher, and H. C. Astley, “Generation of propulsive force via vertical undulations in snakes,” *J. Exp. Biol.*, vol. 224, no. 13, 2021.

[43] H. F. Brinson and L. C. Brinson, *Polymer engineering science and viscoelasticity: An introduction, Second edition*. 2015.

[44] T. Soderstrom and P. Stoica, *System identification*. Prentice-Hall International, 1989.

[45] E. R. Cholleti, J. Stringer, P. Kelly, C. Bowen, and K. Aw, “Studying the creep behaviour of stretchable capacitive sensor with barium titanate silicone elastomer composite,” *Sensors Actuators, A Phys.*, vol. 319, p. 112560, 2021.

[46] T. Li, B. Jayawardhana, A. M. Kamat, and A. G. P. Kottapalli,

“Source-Seeking Control of Unicycle Robots With 3-D-Printed Flexible Piezoresistive Sensors,” *IEEE Trans. Robot.*, pp. 1–15, 2021.

[47] Q. Fu and C. Li, “Snake robot traversing large obstacles using vertical bending with contact force feedback,” *IEEE Int. Conf. Robot. Autom., Submitted*

https://youtu.be/R1_FxCMab-0